JMEPEG (2012) 21:2460–2466
DOI: 10.1007/s11665-012-0194-3

1059-9495/$19.00

Kinetic Study of the Austempering Reactions in Ductile Irons

M.J. Pérez, M.M. Cisneros, E. Almanza, and S. Haro

(Submitted April 8, 2011; in revised form January 24, 2012)

Kinetics of the reaction that occur during the austempering heat treatment in unalloyed and alloyed ductile irons with 1Cu-0.25Mo, 1Ni-0.25Mo, and 0.7Cu-1Ni-0.25Mo, was studied. The austenitization and austempering cycles were achieved by isothermal dilatometry in cylindrical samples of 2 mm in diameter and 12 mm in length. The specimens were austenitized at 870 °C for 120 min, followed by isothermal holding for 300 min at temperatures between 270 and 420 °C. Kinetic parameters such as the order of reaction "*n*" and the rate of reaction "*k*" were calculated using the Johnson-Mehl equation while the empirical activation energy was calculated by means of the Arrhenius equation. It was found that the values of "*k*" decreased with the addition of Cu, Ni, and Mo as well as with the reduction of the isothermal temperature. The activation energy changes with the austempering temperature, in the range 30,348-58,250 J/mol when the heat treatment was carried out between 370 and 420 °C and 10,336-26,683 J/mol when the temperature varied from 270 to 350 °C. The microstructures in samples austempered at 370 and 315 °C were observed by transmission electron microscopy. No carbides precipitation was observed on samples heat treated at 370 °C for less than 120 min, while at 315 °C carbides of hexagonal structure ε($Fe_{2.4}C$) were found from the beginning of the transformation. The smallest value of activation energy and a slower kinetic transformation seem to be related with the presence of a carbide phase. Additionally, the time results obtained for transformation fractions of 0.05 and 0.95 by the dilatometry analysis were used to build the temperature-time-transformation diagrams for the irons.

Keywords austempering, ductile iron, kinetic parameters, TTT diagrams

1. Introduction

Ductile irons can be considered as a ternary alloy of Fe-C-Si. These alloys are well known for their low production cost, good recycling capacity, excellent castability and a wide range of mechanical properties that depend on the size, form, and distribution of graphite and metallic matrix. The production and applications of ductile irons have increased in recent years, in particular for the automotive industry replacing wrought steels and some aluminum alloys (Ref 1, 2). This tendency is associated with the development of new technologies such as austempered heat treatment applications that produce more than twice the strength for a given level of ductility compared with conventional ductile iron (Ref 3-5), as well as the fabrication of thin wall ductile irons that are characterized by higher strength/weight ratio, making them a strong competitors for low-density alloys (Ref 5-7).

The relevant properties of austempered ductile irons (ADI) are obtained by the decomposition, in isothermal conditions, of the high temperature austenite (γ) according to reaction I: $\gamma = \alpha + \gamma_{HC}$. The product of this reaction is a mixture of ferrite (α) and high carbon austenite (γ_{HC}), known as ausferrite (Ref 8). γ_{HC} is not able to hold carbon in solution for a long time at isothermal temperature and it allows the precipitation of carbides (*C*) through reaction II: $\gamma_{HC} = \alpha + C$. This last reaction leads to a detrimental effect on the mechanical properties, mainly on ductility and toughness.

The development of a fully ausferritic structure is the goal of austempering heat treatment. It is necessary to know the temperature and time conditions to maximize the advance of reaction I while minimizing reaction II, in order to obtain optimal mechanical properties. Many studies have been performed to investigate the effects of heat treatment parameters and chemical composition on the mechanical behavior of austempering irons (Ref 5, 7, 9, 10), but the information that correlates the effects of these parameters with the transformation kinetics of austenite is scarce (Ref 11).

The aim of the present work was to study the kinetics of the reaction $\gamma = \alpha + \gamma_{HC}$ in unalloyed and alloyed (Cu-Mo, Ni-Mo, Cu-Ni-Mo) ductile irons by isothermal dilatometry. The results are used to calculate the kinetics parameters and to construct TTT diagrams in the temperature range between 270 and 420 °C.

2. Experimental Procedure

Ductile irons of compositions given in Table 1 were melted in a induction furnace using steel scrap, ductile iron return, graphite, ferrosilicon (75%Si), ferromolybdenum (65%Mo), electrolytic Ni and Cu as raw materials. The melt was treated

M.J. Pérez, M.M. Cisneros, and **E. Almanza**, Departamento de Posgrado e Investigación, Instituto Tecnológico de Saltillo, Saltillo, Mexico; and **S. Haro**, Unidad Académica de Ingeniería, Universidad Autónoma de Zacatecas, Zacatecas, Mexico. Contact e-mail: mjperez@its.mx.

Table 1 Chemical composition of ductile cast irons

Element, wt.%	Unalloyed (H1)	1Cu-0.25Mo (H2)	1Ni-0.25Mo (H3)	0.7Cu-1Ni-0.25Mo (H4)
C	3.716	3.692	3.877	3.645
Si	2.263	2.488	2.377	2.233
Mn	0.237	0.255	0.318	0.257
S	0.027	0.009	0.012	0.016
P	0.017	0.021	0.024	0.024
Mg	0.031	0.041	0.045	0.047
Cu	…	1.011	…	0.657
Mo	…	0.255	0.242	0.262
Ni	…	…	1.009	1.019
Sn	0.008	0.007	0.007	0.007
Ti	0.003	0.003	0.002	0.003
Al	0.004	0.002	0.004	0.003

Table 2 Phase composition and characteristics of as-cast ductile irons

Structural features	H1	H2	H3	H4
Ferrite, %	65.4	…	63.2	22.7
Pearlite, %	25.7	89.8	26.8	67.8
Graphite, %	8.9	9.7	9.6	9.0
Carbide, %	0	0.5	0.4	0.5
Nodule count, mm^{-2}	165	245	205	155
Nodularity, %	88	95	90	90

with 1.5-1.8% of Fe-Si-Mg alloy (43-48% Si, 4.5-5.5% Mg, 1.5-2.5% Ca) using a tundish cover process. Inoculation treatment in the pouring ladle was carried out by adding 0.35% Fe-Si alloy (74-79% Si, 0.8-1.2% Ca, 0.8-1.2% Ba, 1.5% max of Al). All compositions are in wt.%, and were provided by the supplier. The metal was poured in silica sand molds with Y-blocks impression, according to ASTM-897M (Ref 12). The variation of sulphur content in the final chemical composition (Table 1) is related with the amount of Fe-Si-Mg alloy. The H1 ductile iron was treated with 1.5 wt.% of this ferroalloy.

The proportion of phases present, graphite nodularity, and the nodule count for the as cast irons are given in Table 2. The pearlite over ferrite ratio is a function of the amount of Cu and Mn which promotes a pearlite structure during solidification. The presence of a few intercellular carbides was only detected in alloyed ductile iron. The graphite nodularity was higher than 88%, the remnant was vermicular graphite; laminar graphite was absent. The average nodule count was between 165 and 245 nodules/mm^2. Dilatometric analyses were performed in cylindrical samples of 2 mm in diameter by 12 mm in length. The samples were austenitized at 870 °C in vacuum for 120 min using a heating rate of 0.03 °C/min. The rapid cooling to the austempering temperatures of 420, 400, 370, 350, 315, 300, or 270 °C was achieved by high pressure argon jet on the surface of the specimens. The austempering cycle was completed by cooling to room temperature after 300 min at the treatment temperatures. In addition, samples of 25 × 25 × 6 mm were austenitized at 870 °C for 120 min and then austempered in a molten salt bath for 10, 60, 120, 300, and 1440 min at 370 and 315 °C. These cycles were finished by quenching the samples in water at room temperature. The changes in microstructures were observed by transmission electron microscopy (TEM).

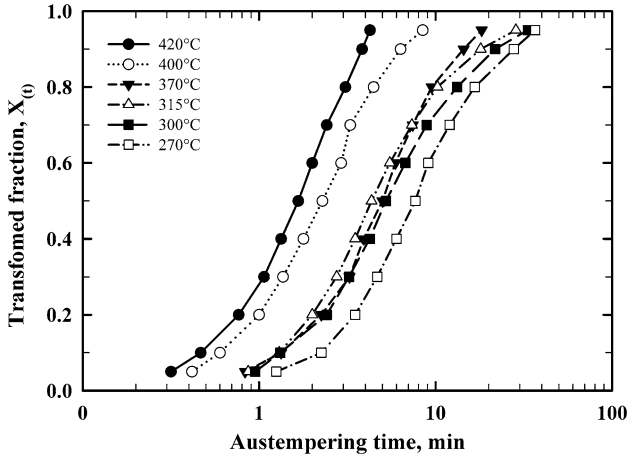

Fig. 1 Influence of austempering temperature on transformed fraction for unalloyed ductile iron H1

3. Results and Discussion

3.1 Kinetic Parameters

A kinetic study of the transformation of austenite (reaction I) in isothermal conditions can be realized considering that the advance of the reaction is proportional to the dilatation observed; the transformation fraction can be defined as: realize

$$X_{(t)} = (L_t - L_0)/(L_f - L_0) = \Delta L_{(t)}/\Delta L_{\max} \quad \text{(Eq 1)}$$

where $\Delta L_{(t)}$ is the dilatation obtained in a time "t" and $\Delta L_{máx}$ represents the dilatation value when the reaction is finished, in other words, the estimated maximum value corresponds to a 100% of decomposition. Also, the transformation rate is proportional to the change in dilatation:

$$V_{(t)} = dX/dt = (1/\Delta L_{\max})(dL/dt) \quad \text{(Eq 2)}$$

The influence of the austempering temperatures and the effect of the alloying elements on the kinetic reaction are shown in Fig. 1. The curves of the transformed fraction are of sigmodial shape, which are characteristics of a diffusive process of nucleation and growth.

The results show that, within the temperature range studied, the rate of transformation is reduced as the holding temperature diminishes (Fig. 1). Although, at low austempering temperatures the driving force for the reaction is higher, the lower diffusivity of carbon in austenite will reduce the transformation kinetics. A slower kinetic is characterized by longer time of incubation at the beginning of the reaction and a long time interval to complete it. Figure 2 shows the curves of transformed fraction for unalloyed and alloyed ductile irons. It is observed that the addition of alloying elements delays the transformation kinetics. In other words, the curves are displaced to the right with respect to the unalloyed ductile iron.

The kinetics of transformation that takes place by nucleation and growth can be described by the Johnson-Mehl equation:

$$X(t) = 1 - \exp(-(kt)^n) \quad \text{(Eq 3)}$$

where "t" is the time of transformation, "k" is a reaction rate constant and it has dimensions of $(\text{time})^{-1}$, "n" is another constant (order of reaction), which is independent of temperature, but it depends on the nucleation and growth processes.

Examples of straight lines obtained by lineal regression of Eq 3 are presented in Fig. 3 for the austempered irons at 370 °C. The data are adjusted to two different straight lines. The reason of the deviation of the lineal behavior can be attributed to the heterogeneity of the eutectic cell, as it can be considered that reaction I proceeds in a relatively homogeneous way at the inside of the eutectic cell when the transformed fraction $X_{(t)}$ remains below a fraction close to 0.7, and the data follows a lineal relationship. Segregation at the intercellular region of elements such as Mo and Mn, which promote the formation of carbides, reduces the diffusivity of carbon and the growth rate of ausferrite structure decreases. This effect is shown in the deviation on the straight line when the transformed fraction is higher than 0.7 (Fig. 3).

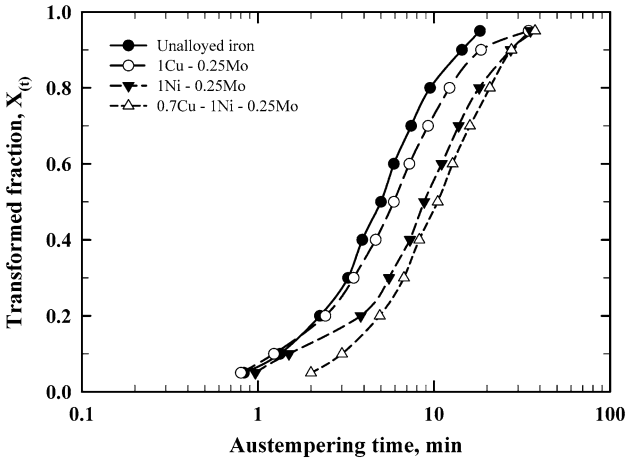

Fig. 2 Sigmoidal curves for ductile irons during austempering at 370 °C

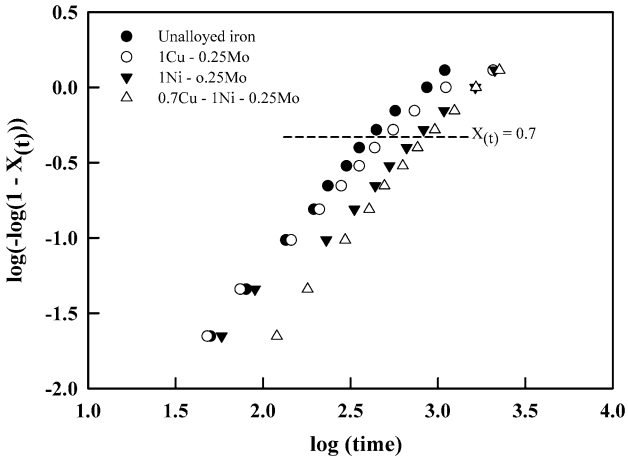

Fig. 3 Plot $\log(-\log(1-X_{(t)}))$ vs. $\log t$ for ductile irons austempered at 370 °C

The "n" and "k" values for the irons at different austempering temperatures are summarized in Table 3. It can be appreciated that the values of exponent "n" are between 1.14 and 1.56, without any significant effect of either the austempering temperature and chemical composition of ductile iron. These results correspond to a localized nucleation and a controlled transformation by the interface reaction (Ref 13). Also, it is observed in Table 3 that the values of "k" decrease when the isothermal temperature decreases and the content of Ni, Cu, and Mo increase.

The activation energy (Q) for the reaction I: $\gamma = \alpha + \gamma_{HC}$, can be calculated by the Arrhenius equation (plotting log k vs. $1/T$), as shown in Fig. 4. The best fit of the data was obtained

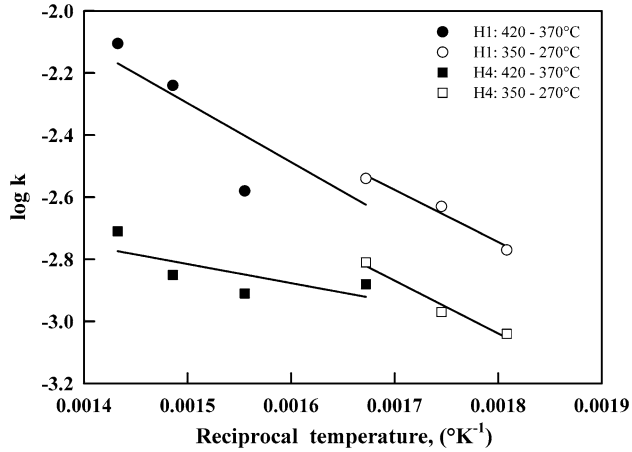

Fig. 4 Plot log k vs. $1/T$ to determine the activation energy of the reaction $\gamma \rightarrow \alpha + \gamma_{HC}$ for H1 and H4 ductile irons

Table 4 Activation energy values for the reaction $\gamma \rightarrow \alpha + \gamma_{HC}$

Austempering temperature, °C	Q, J/mol			
	H1	H2	H3	H4
420-370	58,250	57,187	46,453	30,348
350-270	25,405	26,683	10,336	14,186

Table 3 Influence of austempering temperature on the order of reaction (n) and rate reaction (k) values

Austempering temperature, °C	H1		H2		H3		H4	
	n	$k \times 10^{-4}$, s^{-1}	n	$k \times 10^{-4}$, s^{-1}	n	$k \times 10^{-4}$, s^{-1}	n	$k \times 10^{-4}$, s^{-1}
420	1.53	79.3	1.56	49.1	1.25	24.6	1.14	19.6
400	1.47	57.6	1.25	34.8	1.23	20.2	1.23	14.2
370	1.45	26.8	1.27	21.2	1.15	13.3	1.50	12.4
350	1.41	26.9	1.45	26.8	1.38	15.6	1.32	13.1
315	1.48	28.8	1.48	22.9	1.53	17.4	1.35	15.5
300	1.40	23.4	1.44	19.3	1.43	16.2	1.33	13.5
270	1.45	16.8	1.37	12.6	1.50	12.2	1.44	9.01

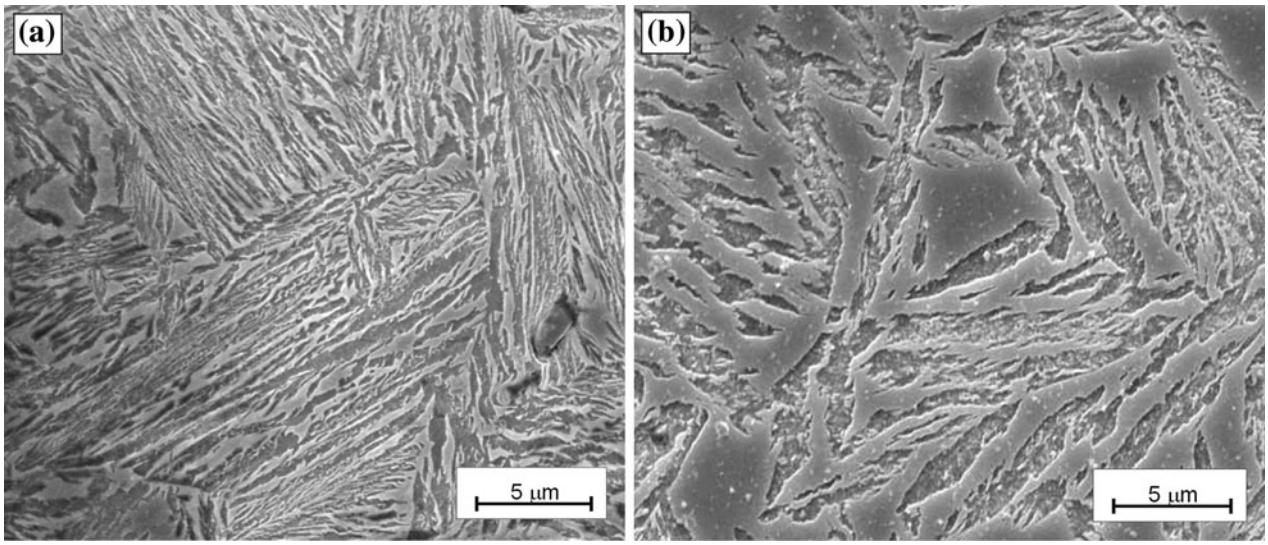

Fig. 5 SEM micrographs of 1Ni-0.25Mo iron austempered for 120 min at (a) 315 °C and (b) 370 °C

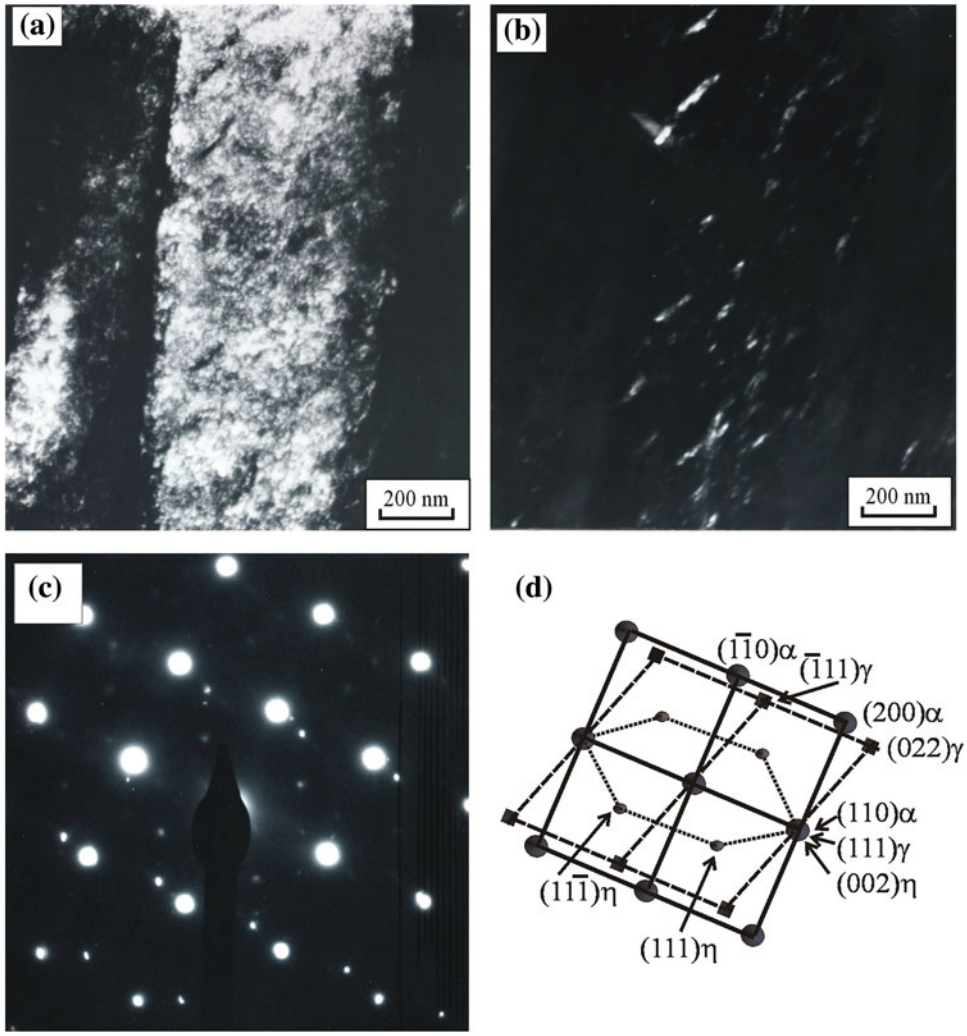

Fig. 6 TEM images of 0.7Cu-1Ni-0.25Mo austempered at 370 °C for 120 min: (a) bright field image, (b) dark field using (111)η reflection, (c) electron diffraction pattern, and (d) indexed diffraction pattern

when separating them into two groups, each group representing its regression line. The discontinuity on straight line appears near 350 °C. The values of Q from this analysis are summarized in Table 4.

The existence of two values of empirical activation energy for the reaction I in the interval between 270 and 420 °C suggests that there is a different contribution of the process involved in the transformation. The experimental evidence in this work shows that ausferrite growth rate is controlled by carbon diffusion. The activation energy values (10,336-26,683 J/mol) found at low temperatures (<350 °C) are related with a low carbon diffusivity that favors the refinement of the microstructure, a smaller portion of high carbon austenite and the precipitation of carbides occurring from the beginning of treatment. In contrast, when the austempering takes place at temperatures above 350 °C, the extent of undercooling diminishes and the diffusivity of carbon increases. As a result there is a coarse microstructure, a greater portion of high carbon austenite and the absence of a carbide phase for short treatment time. In this case the values of Q (30,348-58,250 J/mol) are higher than those found at low temperatures.

3.2 Microstructures

Representative microstructures corresponding to the austempering treatments at 315 and 370 °C are shown in Fig. 5(a) and (b), both microstructures consist of a mixture of acicular ferrite and high carbon austenite. The lower austempering temperature produces an enhanced nucleation rate that results in a highly refined ausferrite (Fig. 5a). It was found that the maximum volume fraction of high carbon austenite was of the order 0.18 during isothermal holding at 315 °C for 120 min. In contrast, when the austempering takes place at higher temperatures (>350 °C) a coarse structure is obtained (Fig. 5b) with an increased of volume fraction of high carbon austenite in the order of 0.34.

Analysis of the microstructure by TEM revealed that the precipitation of carbide phases is a function of the temperature and time of austempering. The microstructure of H2, H3, and H4 irons was free of carbides when treated for less than 120 min at 370 °C, but the presence of small particles localized at the inner of the ferrite needles or at the α/γ interface (Fig. 6) was detected when the irons were austempered for more than

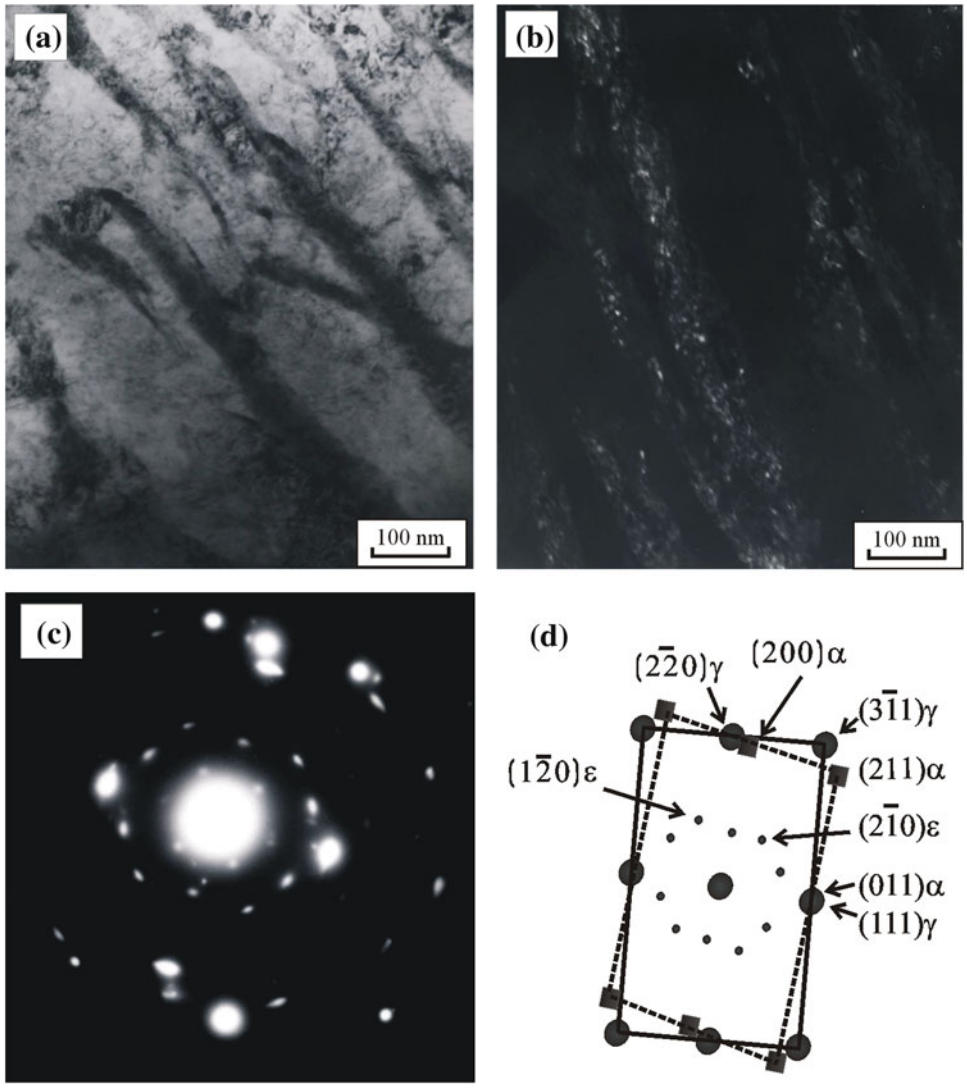

Fig. 7 TEM images of 0.7Cu-1Ni-0.25Mo austempered at 315 °C for 1440 min: (a) bright field image, (b) dark field using (2 $\bar{1}$0)ε reflection, (c) electron diffraction pattern, and (d) indexed diffraction pattern

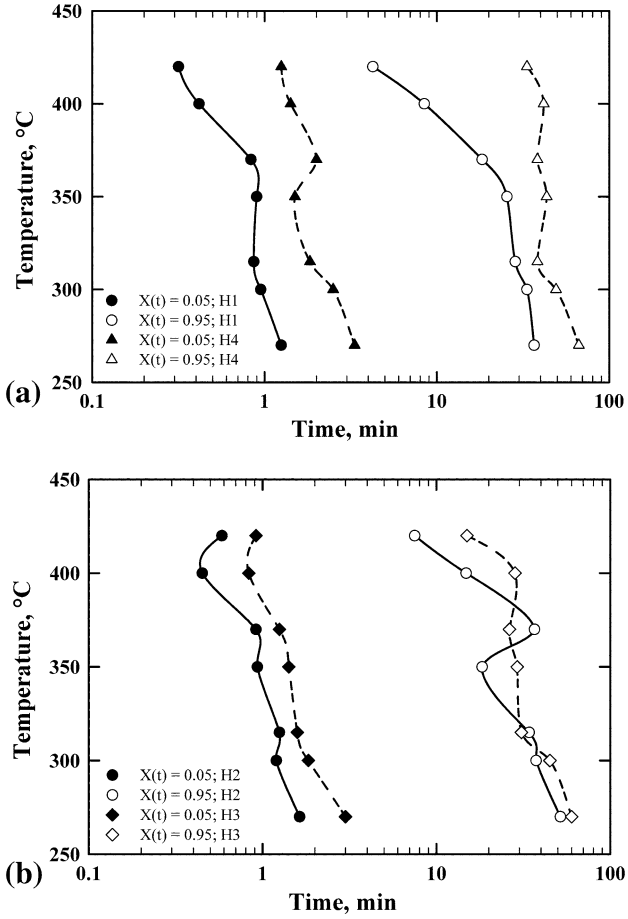

Fig. 8 TTT diagrams: (a) H1 and H4 ductile irons and (b) H2 and H3 ductile irons

120 min. These precipitates were identified as orthorhombic η-Fe_2C carbides. In this case, the austempering conditions and the presence of alloying elements probably delayed the development of reaction II. Precipitation of this carbide has been reported previously, however it changes to χ-carbides after 5 h of treatment at temperatures above 350 °C (Ref 14). The results obtained in this work by TEM reveal that the η-Fe_2C carbides persist after a long time treatment (1440 min). Precipitation of hexagonal ε-$Fe_{2.3}C$ carbides is preferentially located inside the ferrite needles; it is produced by simultaneous development of the reactions $\gamma \rightarrow \alpha + \gamma_{HC}$ and $\gamma_{HC} \rightarrow \alpha + C$, and it was observed to occur at all times of austempering at 315 °C for unalloyed and alloyed ductile iron and in the unalloyed ductile iron (H1) at 370 °C (Fig. 7). Precipitation of ε-carbide has been reported only in unalloyed ductile irons being austempered at 300 °C after 1 h of treatment (Ref 15). In this research, the small values of the activation energy and the slow transformation kinetics at 315 °C, could be due to the presence of ε carbide from the beginning of the reactions.

3.3 TTT Diagrams

The experimental time to obtain the transformation fractions of 0.05 and 0.95 from the isothermal dilatometry curves were used to build the TTT diagrams for each iron (Fig. 8). TTT diagrams show two defined zones, one between 420 and 370 °C and the other zone in the interval of 350 and 270 °C. Each zone is associated with the formation of a product with different morphology according to austempering temperature and a different kinetic transformation. In general, the TTT diagrams show that a decrease in the isothermal temperature reduces the kinetics of the reaction illustrated by an increase in the time both at the beginning and at the end of the reaction I ($\gamma = \alpha + \gamma_{HC}$), due to a reduction in the diffusion of carbon. A simple calculation of the carbon diffusion in ferrite shows that this is reduced from 1×10^{-8} to 9.8×10^{-10} cm^2/s at 400 and 300 °C, respectively. The presence of alloying elements in the iron promotes slower kinetics of reaction that is manifested by a displacement of the curves towards the right. At higher amounts of alloying elements displaces the start of reaction toward higher time (Fig. 8a). The onset of the reaction is slower with the addition of 1% Ni than with 1% Cu for the same amount of Mo (0.25), Fig. 8(b).

4. Conclusions

1. The rate of isothermal transformation $\gamma = \alpha + \gamma_{HC}$ decreases with the time, particularly after 0.7 of transformed fraction. The reason for deviation from the lineal behavior is the compositional inhomogeneity of the eutectic cells. This segregation is not removed during austenitization.
2. The activation energy (Q) is in the range 30,348-58,250 J/mol for the irons heat treated at 420 to 370 °C, while the activation energy for temperatures in the range 350-270 °C is on the order of 10,336-26,683 J/mol. The Q values depend on the atomic processes involved in the kinetics of transformation.
3. Observations using TEM showed the presence of a fine dispersion of ε-$Fe_{2.3}C$ carbides on the inside of the needles of ferrite for short-time treatment for all irons austempered at 315 °C and unalloyed iron austempered at 370 °C. At high temperatures (370 °C), the presence of η-Fe_2C carbides was detected after 120 min of austempering, only in alloyed ductile iron.
4. Two well-defined zones are shown on the isothermal transformation diagrams; coarse ausferrite is obtained in the high temperature zone (370-420 °C) and a refined structure is obtained in the lower temperature zone (350-270 °C).
5. The chemical composition has a significant effect upon the relative position in time of the transformation curves in TTT diagrams. All the curves were displaced to the right by the presence of the alloying elements.

References

1. K.L. Hayrynen and J.R. Keough, The Status of Austempered Cast Irons in 2007, *AFS Trans.*, 2008, **116**, p 747–757
2. American Foundry Society, 43rd Census of World Casting Production 2008, *Mod. Cast.*, 2009, **98**(12), p 17–21
3. M.F. Hafiz, Tensile and Impact Properties of Conventional and Austempered SG-Cast Irons, *AFS Trans.*, 2009, **117**, p 445–452
4. K. Hanzlikova, S. Véchet, and J. Kohout, Influence of Microstructure Composition on Mechanical Properties of Austempered Ductile Iron, *Kovove Mater.*, 2008, **46**, p 117–121
5. D.M. Stefanescu, R. Ruxanda, and L.P. Dix, The Metallurgy and Tensile Mechanical Properties of Thin Wall Spheroidal Graphite Irons, *Int. J. Cast Metals Res.*, 2003, **16**(1–3), p 319–324

6. A.P. Druschitz and D.C. Fitsgerald, Lightweight Iron and Steel Casting for Automotive Applications, *2000 SAE World Congress*, Detroit, Michigan, USA, 2000, p 1–8
7. M.M. Mourad, K.M. Ibrahim, and A.A. Nofal, Optimizing the Properties of Thin Wall Austempered Ductile Iron, *68th World Foundry Congress*, Chennai, India, 2008, p 161–166
8. "Terminology Relating to Iron Casting", A 644, Annual book of ASTM Standards, Part 1, *ASTM*, p 333–334
9. C. Valdés, M.J. Pérez, M. Figueroa, and L.E. Ramirez, Austempered Ductile Iron with Dual Matrix Structures, *Rev. Mex. Fís.*, 2009, **55**, p 48–51
10. J. Zimba, D.J. Simbi, and E. Navara, Austempered Ductile Iron: An Alternative Material for Earth Moving Components, *Cem. Concr. Compos.*, 2003, **25**, p 643–649
11. M. Nili-Ahmadabadi and S. Farjami, Application of Computational Thermodynamics and Kinetic to Control of High Mn Ductile Iron Austempering, *Int. J. Cast Metals Res.*, 2003, **16**(1–3), p 71–75
12. "Specification for Austempered Ductile Iron Castings", A 897, Annual book of ASTM Standards, Part 1, *ASTM*, p 557–562
13. J.W. Chistian, *The Theory of Transformation in Metals and Alloys*, 3rd ed., Pergamon Press, Oxford, 2002, p 538–546
14. L. Sidjanin, R.E. Smallman, and J.M. Young, Electron Microstructure and Mechanical Properties of Silicon and Aluminum Ductile Irons, *Acta Metall. Mater.*, 1994, **42**, p 3149–3156
15. L. Sidjanin and R.E. Smallman, Metallography of Bainitic Transformation in Austempered Ductile Iron, *Mater. Sci. Technol.*, 1992, **8**, p 1095–1103